J Neurophysiol 106: 1604–1613, 2011.
First published July 6, 2011; doi:10.1152/jn.00126.2011.

Expression patterns of nicotinic subunits $\alpha2$, $\alpha7$, $\alpha8$, and $\beta1$ affect the kinetics and pharmacology of ACh-induced currents in adult bee olfactory neuropiles

Julien Pierre Dupuis, Monique Gauthier, and Valérie Raymond-Delpech
Université de Toulouse, UPS, Centre de Recherches sur la Cognition Animale (CRCA), CNRS UMR 5169, Toulouse Cedex, France

Submitted 16 February 2011; accepted in final form 5 July 2011

Dupuis JP, Gauthier M, Raymond-Delpech V. Expression patterns of nicotinic subunits $\alpha2$, $\alpha7$, $\alpha8$, and $\beta1$ affect the kinetics and pharmacology of ACh-induced currents in adult bee olfactory neuropiles. *J Neurophysiol* 106: 1604–1613, 2011. First published July 6, 2011; doi:10.1152/jn.00126.2011.—Acetylcholine (ACh) is the main excitatory neurotransmitter of the insect brain, where nicotinic acetylcholine receptors (nAChRs) mediate fast cholinergic synaptic transmission. In the honeybee *Apis mellifera*, nAChRs are expressed in diverse structures including the primary olfactory centers of the brain, the antennal lobes (ALs) and the mushroom bodies (MBs), where they participate in olfactory information processing. To understand the nature and properties of the nAChRs involved in these processes, we performed a pharmacological and molecular characterization of nAChRs on cultured Kenyon cells of the MBs, using whole cell patch-clamp recordings combined with single-cell RT-PCR. In all cells, applications of ACh as well as nicotinic agonists such as nicotine and imidacloprid induced inward currents with fast desensitization. These currents were fully blocked by saturating doses of the antagonists α-bungarotoxin (α-BGT), dihydroxy-β-erythroidine (DHE), and methyllycaconitine (MLA) (MLA $\geq$ α-BGT $\geq$ DHE). Molecular analysis of ACh-responding cells revealed that of the 11 nicotinic receptor subunits encoded within the honeybee genome, $\alpha2$, $\alpha8$, and $\beta1$ subunits were expressed in adult Kenyon cells. Comparison with the expression pattern of adult AL cells revealed the supplementary presence of subunit $\alpha7$, which could be responsible for the kinetic and pharmacological differences observed when comparing ACh-induced currents from AL and Kenyon cells. Together, our data demonstrate the existence of functional nAChRs on adult MB Kenyon cells that differ from nAChRs on AL cells in both their molecular composition and pharmacological properties, suggesting that changing receptor subsets could mediate different processing functions depending on the brain structure within the olfactory pathway.

antennal lobe cells; Kenyon cells; patch clamp; single-cell reverse transcriptase-polymerase chain reaction

NICOTINIC ACETYLCHOLINE RECEPTORS (nAChRs) are abundant within the central nervous system of insects, where they mediate fast excitatory neurotransmission. Native neuronal nAChRs have been described in several insect species such as cockroaches (Salgado and Saar 2004), locusts (Hermsen et al. 1998), crickets (Cayre et al. 1999), houseflies (Jepson et al. 2006), moths (Vermehren and Trimmer 2005), and honeybees (Barbara et al. 2005; Goldberg et al. 1999; Wüstenberg and Grünewald 2004). Despite common properties such as cation selectivity and inward rectification, pharmacological characterization of these receptors has brought to light striking differences from mammalian nAChRs, a crucial point since it confers a remarkable selectivity for neonicotinoids, the major class of synthetic insecticides.

In vertebrates, nAChRs are pentameric membrane proteins belonging to the dicysteine-loop ("cys-loop") superfamily of ligand-gated ion channels (LGICs) including both cation- and anion-permeable channels (Raymond and Sattelle 2002). Each subunit possesses four transmembrane domains (M1–M4), an extracellular amino-terminal domain involved in agonist binding, and a large phosphorylable cytoplasmic loop between M3 and M4 involved in receptor assembly and regulation in mammals (for review see Albuquerque et al. 2009; Thany et al. 2007). The ion pore is created by the M2 transmembrane segments and defines channel gating properties, ion selectivity, and conductivity. So far, complete insect cys-loop LGIC superfamilies have been described in *Drosophila* (Dent 2006), honeybee (Jones and Sattelle 2006), and red flour beetle (Jones and Sattelle 2007), the honeybee genome containing 21 candidate subunits. Among these 21 members, 11 orthologs of known *Drosophila* nAChR subunits—9 α and 2 β—have been reported (Jones and Sattelle 2006) that potentially enter into the yet-unknown molecular composition of honeybee nAChRs. If subunits Amelα5, Amelα6, and Amelα7 share 34%, 44%, and 40% identity, respectively, with the vertebrate $\alpha7$ subunit, several honeybee subunits do not have clear vertebrate homologs and therefore have been named after their *Drosophila* counterparts (Jones et al. 2006). However, their respective functional roles remain poorly defined.

Immunocytochemical and electrophysiological studies have shown that major networks of the honeybee brain are cholinergic, including structures involved in the processing of olfactory information such as the antennal lobes (ALs), the primary olfactory neuropile of the brain, and the mushroom bodies (MBs) (Barbara et al. 2008; Bicker 1999; Wüstenberg and Grünewald 2004). Olfactory sensory neurons located in the antennae send cholinergic inputs to the AL neurons, namely, local interneurons and projection neurons (PNs), with which they interact within the glomeruli constituting the AL external layout (Kelber et al. 2006; Fig. 1). After a first processing step in the AL, cholinergic PNs send the information to the calyces of the MBs where they synapse onto Kenyon cells (KCs), which perform a final integration of olfactory, visual, and gustatory signals (Brandt et al. 2005). Thus AL cells and KCs

Address for reprint requests and other correspondence: V. Raymond-Delpech, Université de Toulouse, UPS, Centre de Recherches sur la Cognition Animale (CRCA), CNRS UMR 5169, 118 route de Narbonne, F-31062 Toulouse Cedex 9, France (e-mail: raymond@cict.fr).

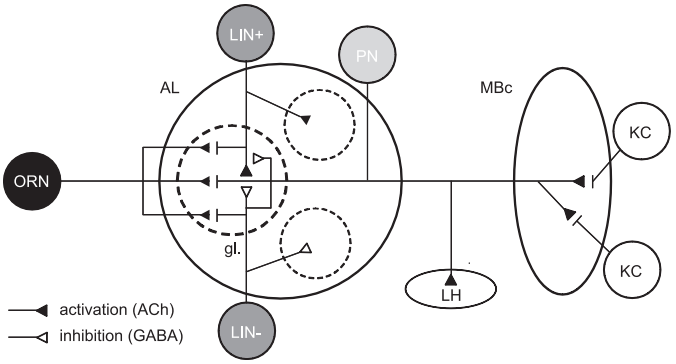

Fig. 1. Schematic representation of a hypothetical architecture of synaptic wiring within the olfactory network of the honeybee, based on the literature. Represented in black is an olfactory receptor neuron (ORN), in dark gray inhibitory and excitatory local interneurons (LIN− and LIN+, respectively), in light gray a projection neuron (PN), and in white 2 mushroom body Kenyon cells (KCs). Dotted circles represent glomeruli (gl.). AL, antennal lobe; MBc, mushroom body calyx; LH, lateral horn; ACh, acetylcholine. Excitatory cholinergic inputs are represented as black filled triangles and major inhibitory inputs (GABAergic) as white triangles.

both receive information in the form of cholinergic inputs and perform two successive steps of olfactory information processing. Interestingly, behavioral studies demonstrated that injecting nicotinic antagonists into the honeybee brain impacts on olfactory memory formation in different ways depending on the nature of the antagonist. Injections of mecamylamine (mammalian heteromeric nAChR antagonist) affect the memory retrieval process (Lozano et al. 2001) and injections of α-bungarotoxin (α-BGT) and methyllycaconitine (MLA; mammalian α7-containing nAChR antagonist) specifically disrupt long-term memory formation, whereas dihydroxy-β-erythroidine (DHE; mammalian $\alpha4\beta2$ nAChR antagonist) injections only affect retrieval after short delays (Gauthier et al. 2006). Cholinergic signaling thus seems to be involved in both memory formation and retrieval via pharmacologically distinct nAChR subtypes potentially distinguishable by their respective sensitivities to α-BGT (Dacher et al. 2005), as is suggested in mammals, where predominant α-BGT-sensitive α7 and -insensitive $\alpha4\beta2$ receptors both play a role in memory (for review see Hogg et al. 2003).

To get a better understanding of cholinergic signaling in the honeybee brain, we characterized and compared the pharmacological and molecular properties of nAChRs from adult AL and MB KCs. Combining electrophysiological and molecular approaches, we established that KCs mainly express nicotinic subunits α2, α8, and β1 and display a fast-desensitizing ACh-induced current type. AL cells exhibit both majority slow-desensitizing and minority fast-desensitizing nicotinic currents and show a similar expression profile except for the supplementary presence of nicotinic subunit α7. These results suggest the existence of structurally and functionally different nAChRs in MB KCs and AL cells that could mirror two steps of olfactory information processing.

MATERIALS AND METHODS

Animal handling and cell preparation. Honeybees (*Apis mellifera*) were housed in a heated hut outside the laboratory. Animal handling and experiments fully conformed to French regulations. Adult honeybees were captured at the top of the hive and anesthetized by cooling at 4°C. MB calyces were dissected and KCs were cultured following a modified version of a protocol originally developed by Kreissl and Bicker (1992). The head capsule was removed in a Leibovitz L15 medium without L-glutamine (Lonza, Verviers, Belgium) supplemented with (in mM) 123 sucrose, 22.2 glucose, 13.9 fructose, and 28.7 proline, with 0.1 g/l streptomycin and 0.2 U/l penicillin (pH 7.2; all chemicals from Sigma, St. Louis, MO, unless otherwise stated). Head glands were removed, and MB calyces were dissected out of the brains. All preparations were made under semi-sterile conditions, i.e., all preparation equipment was sterilized with 70% ethanol and all solutions were filtered. MB calyces were incubated for 20 min at 30°C in a dissociation saline (Cell dissociation solution nonenzymatic 1×; Sigma) supplemented with protease (type IX from *Bacillus polymyxa*) and collagenase (type I from *Clostridium histolyticum*) (1 g/l each). MB calyces were then transferred into supplemented L15 medium and mechanically dissociated by gentle trituration. Aliquots equivalent to two MB calyces were then plated on poly-L-lysine-coated glass coverslips (0.1 g/l poly-L-lysine, mol mass 150–300 kDa, pH 8.5) contained in culture dishes. Cells were allowed to settle and adhere to the substrate for 2 h at 26°C in an incubator at high humidity. The dishes were then filled with 3 ml of culture medium composed of 13% (vol/vol) heat-inactivated fetal calf serum (Lonza, Verviers, Belgium), 1.3% (vol/vol) yeast extract ultrafiltrate 50× (Sigma), 19.1 mM glucose, 11.9 mM fructose, 24.7 mM proline, 125 mM sucrose, 2 mM L-glutamine, and 50 μg/ml gentamicin, completed with L15 medium without L-glutamine (Lonza) adjusted to pH 6.7 with NaOH. Cells were kept at 26°C in an incubator before use for electrophysiological measurements.

AL cells were prepared according to the same protocol except for the enzymatic dissociation step, which was extended to 45 min.

Electrophysiology. Whole cell patch-clamp recordings were performed at room temperature between 24 h and 4 days after cell preparation as previously described (Hamill et al. 1981). Patch pipettes were pulled from borosilicate glass capillaries (1.5 mm OD, 0.86 mm ID; Harvard Apparatus, Les Ulis, France) with a vertical puller (PP-850, Narishige Scientific Instrument Lab, Tokyo, Japan) and had tip resistances between 5 and 10 MΩ. Pipettes contained (in mM) 18.4 KCl, 88.6 K-gluconate, 40 KF, 3 Na_2ATP, 3 $MgCl_2$, 10 HEPES, 120 sucrose, 3 glutathione, 0.1 Na_2GTP, 1 $CaCl_2$, and 10 EGTA (pH 6.7). Glass coverslips containing the attached cells were placed in a RC-25F perfusion chamber (Harvard Apparatus). Cells were bathed in a standard external saline containing (in mM) 130 NaCl, 6 KCl, 4 $MgCl_2$, 5 $CaCl_2$, 10 HEPES, 25 glucose, and 185 sucrose (pH 6.7). Drugs were added as specified. Application of various solutions to the cells was performed with a SF-77B perfusion fast-step system (Harvard Apparatus), enabling a fast solution exchange (<100 ms). Agonists were applied during 2 s with an interval of 25 s to avoid any cumulative receptor desensitization. Membrane potential was held at −110 mV during all experiments except ion permeability determination. Recordings were performed with an Axopatch 200B amplifier (Axon Instruments, Union City, CA) connected to a Digidata 1440A (Axon Instruments) for data digitization. Data acquisition and analysis were carried out with pClamp10 (Axon Instruments). Currents were sampled at 2 kHz and low-pass filtered at 1 kHz.

Concentration-response curves. Concentration-response curves were determined for both nAChR agonists and antagonists. The agonists applied were ACh, nicotine (NIC), and imidacloprid (IMI). All of these were dissolved in the standard external saline. For concentration-response curve determination, agonists were applied during 2 s at various concentrations alternately with a reference pulse (1 mM ACh), always in an increasing concentration order. To compare amplitudes, currents measured in the presence of agonists (I) were normalized to the currents elicited by the reference ACh concentration (I_{max}, 1 mM ACh). Because peak amplitude measurements can sometimes be misleading regarding pharmacological characterization because of rapid desensitization of nAChRs (Papke and Porter Papke 2002), net charge analyses (NCA) were also performed (affinity

values indicated in parentheses). However, since both methods yielded similar results and because most pharmacological studies on insect nAChRs are based on peak amplitude measurements, we chose to refer to peak amplitudes rather than net charge in order to ease comparison with previously described insect nAChRs.

The antagonists applied were MLA, DHE, and α-BGT. All were dissolved in DMSO [final concentration in the standard external saline <0.1% (vol/vol)]. At least two pulses of NIC (1 mM) were performed prior to antagonist application. To obtain inhibition curves, antagonists were applied at various concentrations in an increasing order. Antagonists were applied 30 s (time necessary for maximum inhibition) before reference NIC concentration application (1 mM). Cells were then washed out with standard external saline, and NIC was repeatedly applied until full-amplitude currents were recovered. Subsequently, only if NIC-induced currents fully recovered could further antagonist concentrations be tested. As for agonists, peak amplitudes or net charges were normalized (I/I_{max}) to the current elicited by 1 mM NIC before antagonist application.

For both agonists and antagonists, nonlinear curve fittings were performed with GraphPad Prism Software (GraphPad Software) and OriginLab 8.1 software using the following Hill equation:

$$\Psi = I_{min} + (I_{max} - I_{min})/[1 + 10^{(\log EC_{50} - [X])n_H}]$$

where X is the logarithm of the compound concentration, Ψ is the normalized response, I_{max} and I_{min} are the maximum and minimum normalized responses, respectively, EC_{50} is the concentration giving half-maximal normalized response, and n_H is the Hill coefficient.

Graphical representations were performed with OriginLab 8.1 software. Results are displayed as mean ± standard error of the mean (SE). Error bars in figures represent SE and are only shown if greater than symbols.

Reversal potential determination. The reversal potential for NIC-induced currents was determined by measuring the current amplitudes elicited by 1 mM NIC application at various command potential steps between −110 mV and +30 mV (10-mV step increment). For these experiments, both a standard external saline (130 mM Na^+) and a sodium-depleted external saline (70 mM Na^+), in which sodium was partially removed by replacing 60 mM NaCl by 60 mM Tris chloride (Tris-Cl), were used to evaluate the contribution of sodium ions to NIC-induced currents. The contribution of calcium ions was assessed with the use of two external salines containing 5 mM and 50 mM calcium (calcium increased by adding 45 mM $CaCl_2$, chloride concentration adjusted to 244 mM with Tris-Cl in both external salines), respectively. The reversal potentials were estimated by a nonlinear regression method fitting data near the zero crossing. They were calculated for each cell and averaged between cells. Relative ion permeabilities were determined as previously described (Barbara et al. 2008).

Data analysis and statistics. Currents were low-pass filtered at 100 Hz (Gaussian-type filter) after acquisition whenever appropriate. Data analysis was performed with Clampfit 10.1 (pClamp 10, Axon Instruments). The relative mean peak amplitude of each agonist-induced current was calculated by normalization to the current induced by the application of 1 mM NIC. SE is given throughout the text. The time constant of current desensitization was determined with Clampfit 10.1 (pClamp 10, Axon Instruments). Drug affinities and current amplitudes were compared with a *t*-test, a one-way ANOVA with a Tukey post hoc test, or a Wilcoxon test depending on the number of groups considered. Reversibility of the antagonists was assessed through comparison of the NIC-induced currents before and after the antagonist application by a Wilcoxon test. Statistical analyses were performed with Statistica 5.5 (Statsoft, Tulsa, OK).

Single-cell RT-PCR. Single-cell RT-PCR was performed on AL cells and KCs after electrophysiological recordings 24 h to 4 days after cell preparation, mainly as previously described (Dupuis et al. 2010). Patch pipettes were filled with 8 μl of diethyl pyrocarbonate (DEPC)-treated RT-PCR internal solution (in mM: 140 KCl, 3 $MgCl_2$, 5 EGTA, 10 HEPES). After whole cell patch-clamp recording, the cell cytoplasm was aspirated into the patch pipette. The pipette was removed from the bath, and the cytoplasm was expelled into a PCR tube kept on ice and immediately frozen at −20°C. Unpatched filled pipettes immersed in the cell bath were used as a control. At the end of the patch-clamp experiment RT reactions were performed, following RevertAid First Strand cDNA Synthesis Kit (Fermentas Life Sciences, Burlington, ON, Canada) instructions. After a 5-min step at 25°C allowing random hexamer primers and RNAs to hybridize, the samples were incubated for 1 h at 42°C. A final 5-min step at 70°C was performed to stop the RT reaction.

The RT reaction products (cDNAs) were then used as templates for a first step of PCR amplification. cDNA aliquots (8 μl) were added to a PCR mix to give the following final concentrations: 1× DreamTaq PCR buffer, 50 μM dNTPs, and 5 U/50 μl of DreamTaq Polymerase (Fermentas Life Sciences). This mix was incubated for 1 min at 94°C before addition of each primer at 100 nM to prevent nonspecific reactions. A 10-min step at 94°C allowed the denaturation of newly synthesized RNA/DNA duplex. The samples were then submitted to 35 cycles of amplification (30 s at 94°C, 30 s at 56°C, 1 min 30 s at 72°C), followed by a single extension step of 10 min at 72°C (Flexigene thermal cycler, Techne, Burlington, NJ).

Aliquots (2 μl) of these first-step multiplex PCRs were then used as templates for a second step of nested PCR amplification. For this step, new couples of primers matching inner sequences of the first-step PCR products were designed. This second run was performed essentially as the first, except that only one pair of primers (1 μM each primer) was added per PCR. After this second PCR, 10 μl of each sample was run on a 1% agarose gel, and all RT-PCR products were sequenced to confirm their identity (MilleGen, Labège, France). Eleven genes in the honeybee genome (Honeybee Genome Sequencing Consortium 2006) are known to code for potential nAChR subunits: α1–α9, β1, and β2 (Jones et al. 2006). Therefore, subunit-specific primers were designed to determine the expression of their corresponding transcripts. Primer sequences were used previously (Jones et al. 2006) and are given in Table 1.

RESULTS

Evidence of nAChRs on adult honeybee mushroom body Kenyon cells. Whole cell patch-clamp experiments were performed on cultured MB KCs from adult honeybee brains. Most of the recorded cells (155 of 178) responded with a fast inward current to the application of 1 mM ACh or 1 mM NIC at a holding potential of −110 mV (Fig. 2*B*), pointing out the presence of nAChRs in MB KCs and confirming previous reports on pupal honeybees (Déglise et al. 2002; Goldberg et al. 1999; Wüstenberg and Grünewald 2004). The peak amplitude of the maximum ACh-induced currents ranged between −11.9 pA and −111.7 pA, with a mean peak amplitude of −25.4 ± 2 pA (n = 52). Receptor desensitization was assessed through sustained application of 1 mM ACh (20 s): the decay phases of the ACh currents could be fitted with a single exponential function, yielding a time constant τ of 50.2 ± 4.6 ms (n = 13). Moreover, ACh-induced currents increased in a concentration-dependent manner: the concentration-response curve for ACh yielded an EC_{50} of 35.8 ± 2.7 μM (n_H = 0.59, Fig. 2*A*. Because peak amplitude measurements can sometimes be misleading regarding pharmacological characterization because of rapid desensitization of nAChRs (Papke and Porter Papke 2002), NCAs of ACh-induced currents were also performed, which yielded an EC_{50} of 32.7 ± 5.9 μM (n_H = 0.62). NCA-obtained affinity values are further indicated in parentheses.

Table 1. *Primer pairs designed for RT-PCR*

Primers	Sequence (5′ → 3′) Forward	Reverse	RT-PCR Product Size, bp
Act PCR1	GGAAATGGCAACTGCTGCAT	TCCACATCTGTTGGAAGGTG	395
Act PCR2	CCGTTGTCCCGAGGCTCTTT	GACCCACCAATCCATACGGAA	267
α1 PCR1	ATGGCGACGGCCATTTCC	CTCGACGGAAATGTAGTAG	603
α1 PCR2	ATTTCCTGTCTTGTTGCCC	TGGTCACCTCGTAGTTGC	349
α2 PCR1	AAGCTTCTTCTGATGAGGG	AGGAAGGAATTGTTGCTGG	561
α2 PCR2	GCGCATAAGATGCACGGA	GCCTCGCAGAGAATGATG	440
α3 PCR1	TTATACTTCCGTCGAGTGG	AACGAATGCCTTCGATAGC	863
α3 PCR2	TGCGTAACCGTGGTAGTC	GTCCCGCGAATCGAGAC	324
α4 PCR1	GCAACTTCGAGGTGACCT	CTATTGTGGCGGACAGTTTA	1343
α4 PCR2	ACGAAGGCCACCATCTAC	CACCGCCGTGGTTCCGA	1299
α5 PCR1	TACTTCCATGCATACTCATC	AACAAAGTTACTCGAATTCCG	778
α5 PCR2	AGTGTCGCCCTGTTGGTA	ATCGGCCATTTTCTTATCTC	724
α6 PCR1	CAATGGAACGAGTCCGAG	GGACAGCGTCCGAGGTG	619
α6 PCR2	TGCGGATGAGGGTTTCG	TCGGCATACTTTCTGCAA	512
α7 PCR1	ATGAGATGGAATGTGTCAGA	TCCTTATCACTTGGTCGTG	808
α7 PCR2	GAGTGAGAGACCTCAGGA	ACGAAGTATACAAGGCAGC	755
α8 PCR1	GAAACAAGAAGCTGGTAGC	TTAGAAGTCGCGGCATCC	515
α8 PCR2	CCATGTTGCACAGAACCC	CCATGGTGACATATTATGTG	360
α9 PCR1	TGGCAGAATTCGGCAAGC	AATCCAATATGGCACCTCG	1008
α9 PCR2	ACGACAATGAATTCGGATTC	GGACAAGGCAAGCGAATC	911
β1 PCR1	TATTTGCTCGAGGCTCGG	GCCGCTCTTCCAATAGTC	589
β1 PCR2	ATCTCCGCCGTTTTCTGC	ACACTTGGTCGCCGTTG	499
β2 PCR1	AAACTGTATCTGTTCTGCGA	GCTTGTCAACATAAGCGAG	855
β2 PCR2	ACGACAGGGACATTATTCC	TGCGGCTAGGGCAAGAG	812

Act, actin.

Pharmacology of Kenyon cell nAChRs. A pharmacological approach was adopted to characterize the properties of KC nAChRs. As for ACh, application of nicotinic receptor agonists NIC and IMI onto KCs also elicited inward currents at a holding potential of −110 mV (Fig. 2). NIC (1 mM) induced small inward currents ranging between −18 pA and −92.3 pA, with a mean peak amplitude of −32.7 ± 1.7 pA (n = 126), whereas IMI (100 μM) induced currents ranging between −11.6 pA and −18.3 pA, with a mean peak amplitude of −15.4 ± 1.1 pA (n = 6). EC_{50} and n_H were estimated from concentration-response curves (Fig. 2*A*) and gave the following ranking orders: IMI (211 ± 2.3 nM, n_H = 0.56; EC_{50} = 527 ± 27 nM by NCA) ≥ NIC (3.7 ± 1.1 μM, n_H = 0.54; EC_{50} = 4.18 ± 6.7 μM by NCA) > ACh (35.8 ± 2.7 μM, n_H = 0.59; EC_{50} = 32.7 ± 5.9 μM by NCA) (ACh vs. NIC, P = 0.0020414; ACh vs. IMI, P = 0.001057; NIC vs. IMI, P = 0.8669). IMI is only a partial agonist of nAChRs on KCs since its efficacy in eliciting maximum inward currents was found to be almost half lower than that of ACh (Fig. 2, *B* and *C*). At concentrations of 100 μM, for which both ACh and NIC induced maximum currents, NIC induced 107.6 ± 6.3% (n = 7) and IMI 50.5 ± 4.8% (n = 6) of the maximum ACh-induced currents. The mean peak currents of the maximum agonist-induced currents are summarized in Table 2.

Since NIC elicited larger currents than ACh, NIC was further used to evaluate the activity of nAChR inhibitors. The NIC-induced currents (1 mM NIC) were blocked by application of nicotinic antagonists α-BGT, DHE, and MLA (Fig. 3). At the highest concentration tested, all three of these completely blocked NIC-induced currents. At lower concentrations, a concentration-dependent reduction of the NIC-induced currents was observed. IC_{50} and n_H were estimated from inhibition curves (Fig. 3*A*) and are summarized in Table 2. IC_{50} comparison gives the following inhibition ranking order: MLA (51.4 ± 5.2 nM, n_H = −1.061; IC_{50} = 54.3 ± 9.5 nM by NCA) ≥ α-BGT (101 ± 2.1 nM, n_H = −1.093; IC_{50} = 148 ± 79 nM by NCA) ≥ DHE (256 ± 1.4 nM, n_H = −0.48; IC_{50} = 147 ± 32 nM by NCA) (α-BGT vs. DHE, P = 0.5461; α-BGT vs. MLA, P = 0.8493; DHE vs. MLA, P = 0.2954). Both DHE and MLA had partially reversible inhibitory actions (for 10 μM DHE: P = 0.0796, Z = 1.753, n = 6; for 10 μM MLA: P = 0.0679, Z = 1.826, n = 4), whereas α-BGT was fully reversible (for 10 μM α-BGT: P = 0.1441, Z = 1.460, n = 4).

Relative ion permeabilities. The recordings obtained at different holding potentials (between −110 and +30 mV, 10-mV step increments) showed that depolarization reduced the maximum peak current amplitude (Fig. 4*A*). In standard saline (130 mM Na^+), NIC-induced currents were inward for holding potentials more negative than +20 mV (Fig. 4, *A* and *B*). With a linear regression method, the reversal potential of the NIC-induced currents was estimated at +23.4 ± 1.7 mV (n = 9). Moreover, decreasing the sodium concentration to 70 mM by replacing 60 mM NaCl by 60 mM Tris-Cl shifted the reversal potential to 2.9 ± 0.8 mV (n = 7) and reduced the current amplitude by 42.7 ± 4.9% at a holding potential of −110 mV (n = 7, P = 0.000656, Z = 3.41), indicating that sodium is involved in the NIC-induced currents. An estimate of the sodium-to-potassium permeability ratio (P_{Na}/P_K) under these ionic conditions was made by fitting its value in the GHK constant field relation to the observed reversal potentials, yielding a best agreement with the experimental data when P_{Na}/P_K = 2.45. Increasing the extracellular calcium concentration from 5 mM to 50 mM by adding 45 mM $CaCl_2$ (chloride concentration adjusted to 244 mM with Tris-Cl in both external salines) induced a nonsignificant shift in the reversal potential from 14.4 ± 1.2 mV (n = 5) to 18.1 ± 0.8 mV (n = 5), indicating that KC nAChRs are weakly permeable to calcium, a potential allosteric modulator of ACh-induced

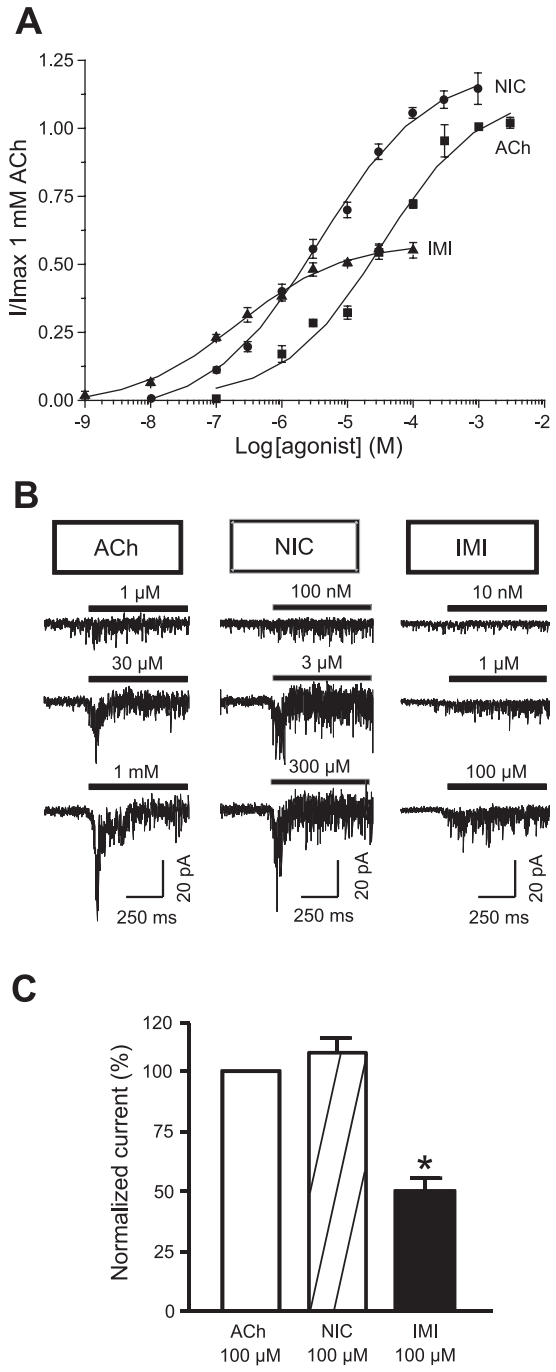

Fig. 2. ACh-induced currents in the mushroom body KCs of the honeybee. *A*: concentration-response curves of nicotinic acetylcholine receptor (nAChR) agonists ACh (■), nicotine (NIC, ●), and imidacloprid (IMI, ▲). Peak current amplitude induced by each agonist concentration was normalized to the maximum elicited current [I/I_{max} (ACh 1 mM)]. Mean ± SE values are plotted (n = 5–13 per point). Smooth lines represent the best fits to the data. EC_{50} and Hill coefficient values were estimated according to the Hill equation. *B*: examples of the agonist-induced currents at the respective concentrations (pulse duration 2 s, holding potential −110 mV). *C*: currents are elicited by the application of ACh, NIC, or IMI (pulse duration 2 s, holding potential −110 mV). Quantification of the peak current amplitudes indicates that the application of 100 μM NIC and IMI induced 107.6 ± 6.3% (n = 7) and 50.5 ± 4.8% (n = 6), respectively, of the 1 μM ACh-induced current. Plotted are the normalized mean peak current amplitudes (relative to the 100 μM ACh-induced current). *$P < 0.05$, significant differences with 100 μM ACh and 100 μM NIC.

currents as suggested in vertebrates (Fig. 4, *C* and *D*). An estimation of the calcium-to-potassium permeability ratio (P_{Ca}/P_K) under these ionic conditions in agreement with experimental data yielded $P_{Ca}/P_K = 0.6$. Ignoring the effects of surface charge, the calcium-to-sodium permeability ratio (P_{Ca}/P_{Na}) was estimated at 0.24.

Molecular composition of AL cell and KC nAChRs. Interestingly, a single type of ACh-induced currents was recorded throughout the patch-clamp experiments performed on KCs, with a desensitization phase that could be fitted with a single exponential function yielding a time constant τ of 50.2 ± 4.6 ms (n = 13, Fig. 5*A*). In contrast, two types of ACh-induced currents coexist in the AL, the primary olfactory neuropile of the honeybee brain, where both majority slow (type I, τ = 539 ± 81 ms; n = 152/170 cells) and minority fast (type II, τ = 32 ± 6 ms; n = 18/170 cells) ACh-elicited conductances were reported (Barbara et al. 2008) as confirmed experimentally (Fig. 5*B*), suggesting the existence of different subsets of nAChRs within these structures of the olfactory pathway.

To better understand the nature of the ACh-gated receptors observed and in order to point out potential differences between nAChRs from KCs and AL cells at the molecular level, we combined single-cell RT-PCR analysis with patch-clamp experiments on both cell populations, following a procedure that allows the simultaneous characterization of the expression of several markers on a single cell (Dupuis et al. 2010). We were able to record from 18 KCs and 26 type I current-displaying AL cells and then apply RT-PCR, all of which were successful as attested by the amplification of our control marker, actin. Using RT-PCR, we also amplified brain tissue transcripts (2 μg) as well as unpatched filled pipettes immersed in the cell bath as controls.

All of the 11 potential nAChR subunit transcripts encoded in the honeybee genome (α1–α9, β1, and β2; Jones et al. 2006) were detected in brain tissue, which served as a positive control, confirming that all 11 nicotinic receptor subunits are expressed in the honeybee brain (Fig. 6*A*). In KCs, however, only α2, α8, and β1 mRNA expression was detected in all cells tested after electrophysiological characterization (Fig. 6*B*). The supplementary presence of α7 mRNAs was also detected in 3 of 18 KCs. Interestingly, the same experiment performed on cultured AL cells yielded a similar expression profile except for the supplementary presence of α7 transcripts in all cells tested (n = 26; Fig. 6*C*). Added to our kinetic and pharmacological observations, these results suggest that both AL cells and KCs potentially express multiple homomeric and/or heteromeric nAChR subtypes based on the unknown association of the subunits described here.

DISCUSSION

Here we show that adult honeybee KCs express functional ACh-gated cationic channels, supporting immunohistochemical reports (Bicker 1999; Thany et al. 2005) as well as electrophysiological studies on pupal honeybees (Goldberg et al. 1999; Wüstenberg and Grünewald 2004). Most of the recorded KCs responded to ACh and nAChR agonists with a fast inward current. Moreover, single-cell RT-PCR analysis coupled with patch clamp indicated that these fast-desensitizing ACh-induced currents potentially rely on the expression of three nAChR subunits, α2, α8, and β1, which possibly associate to

Table 2. *Summary of pharmacological properties*

	ACh, μM	NIC, μM	IMI, nM	DHE, nM	α-BGT, nM	MLA, nM
EC_{50}	35.8 ± 2.7	3.7 ± 1.1	211 ± 2.3			
IC_{50}				256 ± 1.4	101 ± 2.1	51.4 ± 5.2
n_H	0.59	0.54	0.56	−0.48	−1.093	−1.061
Peak current, pA	−25.4 ± 2 (n = 52)	−32.7 ± 1.7 (n = 126)	15.4 ± 1.1 (n = 6)			

Values (means ± SE) are the result of a fit of the data illustrated in Figs. 2, 3, and 4 to the Hill function. Mean ± SE peak currents are given for the agonists acetylcholine (ACh, 1 mM), nicotine (NIC, 1 mM), and imidacloprid (IMI, 1 mM) at the concentration inducing the maximum current. EC_{50}, concentration giving half the maximum normalized activation; IC_{50}, concentration giving half the maximum normalized inhibition; n_H, estimated Hill coefficient; DHE, dihydroxy-β-erythroidine; α-BGT, α-bungarotoxin; MLA, methyllycaconitine.

form homo- and/or heteromeric receptors. Interestingly, our results also point out that the expression patterns of nicotinic subunits in KCs differ from those of AL cells, where the supplementary expression of α7 takes place, which might explain the kinetic and pharmacological differences between the receptor populations.

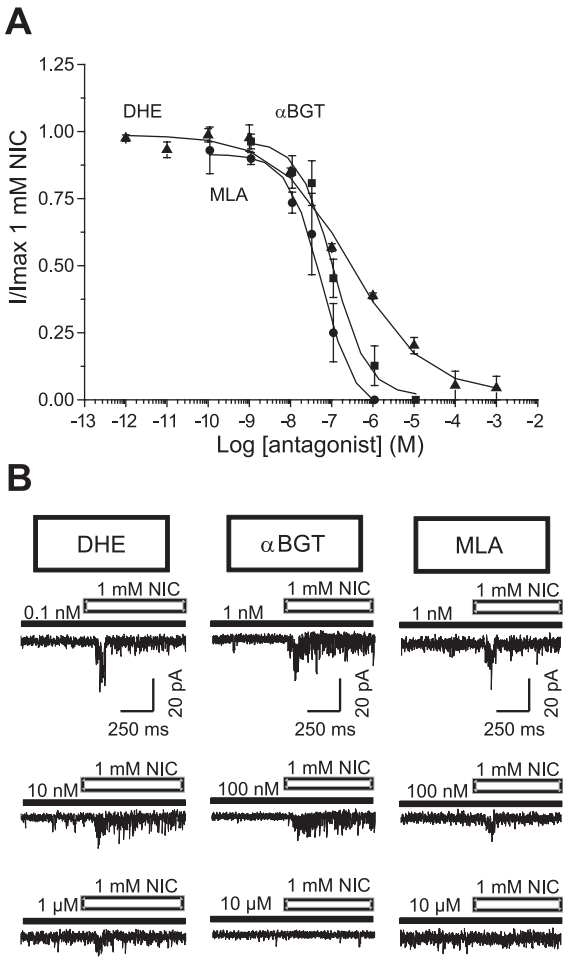

Fig. 3. Concentration-response curves of nAChR antagonists dihydroxy-β-erythroidine (DHE, ▲), α-bungarotoxin (α-BGT, ■), and methyllycaconitine (MLA, ●). *A*: peak current amplitude induced by 1 mM NIC in the presence of each antagonist was normalized to the maximum elicited current [I/I_{max} (NIC 1 mM)]. Mean ± SE values are plotted (n = 4–8 per point). Smooth lines represent the best fit to the data. IC_{50} and Hill coefficient values were estimated according to the Hill equation. *B*: examples of the antagonist-induced inhibition at the respective concentrations (pulse duration 2 s, holding potential −110 mV).

Comparison between nAChRs from AL cells and KCs: molecular implications. The pharmacology of the KC nAChRs is similar to those previously described in other insects (Thany et al. 2007). NIC was found to be a full agonist of KC nAChRs as in cockroach DUM neurons (Lapied et al. 1990) and unlike in honeybee AL cells (Barbara et al. 2008) and other insect preparations, where it acts as a partial agonist (Brown et al. 2006). In contrast, IMI only partially activated KC nAChRs, which is in good accordance with previous reports regarding insect nAChRs (Jepson et al. 2006). Both IMI and NIC displayed comparable EC_{50} values and were more potent than ACh, fitting the previously described properties of adult honeybee AL nAChRs (Barbara et al. 2008), even though IMI and ACh are 10 times more and 2 times less potent in KCs, respectively. ACh and NIC showed very similar n_H values (n_H^{ACh} = 0.59, n_H^{NIC} = 0.54) and comparable efficacies, suggesting a similar mechanism of action for both agonists. These low n_H values contrast with those of vertebrate nAChRs, which are usually between 1 and 2 (Papke and Porter Papke 2002). However, they are consistent with previously reported n_H values of nAChRs in honeybee or other insect neuronal preparations, which range from 0.56 to 1.7 (Albert and Lingle 1993; Barbara et al. 2005, 2008; Déglise et al. 2002; Ihara et al. 2003; Schulz et al. 2000; Shimomura et al. 2005; Wüstenberg and Grünewald 2004), illustrating the diversity of insect nAChRs and the pharmacological distinction from their vertebrate counterparts. All nicotinic antagonists tested on KC nAChRs were effective as in other insect preparations (Cayre et al. 1999; Jepson et al. 2006; Lapied et al. 1990; Salgado and Saar 2004), and all of them shared similar inhibition efficiencies with IC_{50} values ranking within the 100 nM range (MLA, IC_{50} = 51.4 nM; α-BGT, IC_{50} = 101 nM; DHE, IC_{50} = 256 nM). Comparison of n_H values revealed similarities between α-BGT and MLA ($n_H^{\alpha\text{-BGT}} = -1.09$, $n_H^{MLA} = -1.06$) but also a clear dissimilarity with DHE ($n_H^{DHE} = -0.48$), indicating that two different receptor subtypes might be involved in the currents recorded. Interestingly, although nAChRs from adult AL cells share sensitivity to similar antagonists (Barbara et al. 2008), MLA and DHE are 34-fold and 71-fold more potent on AL nAChRs than on KC nAChRs (α-BGT 3-fold less potent on AL nAChRs). Taken together, these results raise the hypothesis that adult AL cells and KCs might contain receptor subtypes displaying different subunit compositions. A similar hypothesis emerges from behavioral studies showing that diverse nAChRs are involved in olfactory learning and memory processes in the honeybee: injecting nicotinic antagonists into the brain impacts olfactory memory formation in different ways depending on the nature of the antagonist, disrupting either memory retrieval (heteromeric-selective antagonist

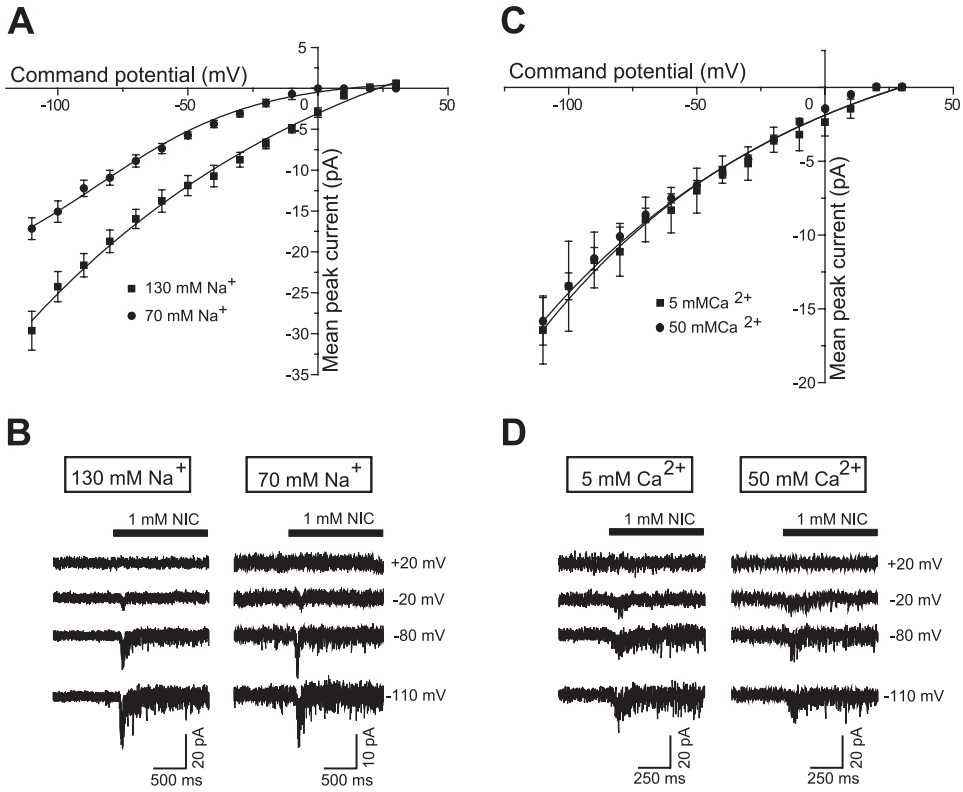

Fig. 4. Reversal potential determination of NIC-induced currents in saline solutions containing different sodium and calcium concentrations. *A*: the NIC-induced currents reversed at +23.4 ± 1.7 mV (n = 9) for 130 mM Na^+ (standard saline). For 70 mM Na^+ (60 mM NaCl substituted by 60 mM Tris-Cl), the reversal potential shifted to 2.9 ± 0.8 mV (n = 7). Mean ± SE values are plotted. *B*: examples of NIC-induced currents recorded at membrane potentials from −110 mV to +30 mV (pulse duration 2 s, 10-mV step increments) in both conditions. *C*: the NIC-induced currents reversed at +14.4 ± 1.2 mV (n = 5) for 5 mM Ca^{2+} (standard saline). For 50 mM Ca^{2+} (45 mM $CaCl_2$ added, chloride concentration adjusted to 244 mM with Tris-Cl as in the standard saline), the reversal potential shifted to 18.1 ± 0.8 mV (n = 5). Mean ± SE values are plotted. *D*: examples of NIC-induced currents recorded at membrane potentials from −110 mV to +30 mV (pulse duration 2 s, 10-mV step increments) in both conditions.

mecamylamine, α4β2-selective antagonist DHE) or long-term memory formation (α7-selective antagonists α-BGT and MLA) (Gauthier et al. 2006; Lozano et al. 2001). Therefore, different nAChR subsets involved in memory processes appear to be expressed within the olfactory pathway of the honeybee, mimicking mammals, in which both homomeric α-BGT-sensitive α7 and heteromeric α-BGT-insensitive α4β2 receptors play a role in memory (Hogg et al. 2003).

When this question was tackled through the combined use of patch-clamp and single-cell RT-PCR, α2, α8, and β1 mRNA coexpression was detected in KCs (Fig. 6*B*). A similar pattern was found in AL cells except for the supplementary presence of α7 transcripts (Fig. 6*C*), potentially explaining the pharmacological differences between AL and KC nAChRs, although this might also rely on varying expression levels or alternative splicing of the same set of nicotinic subunits (Jones et al. 2006). Since a residual α7 expression was observed in 3 of 18 KCs, we cannot exclude that it might also enter the composition of nicotinic complexes in KCs. Considering that three main cell types are colocalized in the calyces of the MBs—outer compact, inner compact, and noncompact KCs, respectively (for review see Farris and Sinakevitch 2003)—we believe that this occasional α7 detection results from KC subtype-specific expression patterns of nicotinic subunits, as previously reported by Thany and collaborators (Thany et al. 2005). On the basis of in situ hybridization experiments, these authors reported that nicotinic subunits α2, α5, and α7 are differentially expressed depending the KC subtypes: α2 and α7 are both expressed in outer compact and inner noncompact KCs, whereas α5 is expressed in outer compact KCs only. Therefore, and since our cell culture protocol does not segregate inner compact KCs from noncompact KCs, we believe that the presence of α7 in 3 of 18 KCs mirrors the expression patterns of two different cell types. One can note that Thany and collaborators reported the supplementary expression of nicotinic subunit α5 in outer compact KCs, which we did not find through single-cell RT-PCR amplification. However, this is not surprising when considering that the KC culture protocol performed here consisted of collecting only the MB calyces, which do not contain the somas of outer compact KCs (Farris and Sinakevitch 2003; Strausfeld 2002). Thus our results unravel the nicotinic subunit expression patterns of either inner compact and/or noncompact KCs of the MB calyces.

Yet the precise stoichiometry of honeybee nAChRs cannot be defined and will require further investigations, although we may hypothesize the presence of α7 homomeric complexes according to pharmacological and molecular homology with vertebrates. However, the molecular composition of honeybee nAChRs might be considerably different from their vertebrate counterparts. Indeed, if Amelα7 shares 40% identity with the vertebrate α7 subunit, Amelα2, Amelα8, and Amelβ1 lack clear vertebrate homologs (Jones et al. 2006). Nevertheless, their *Drosophila* counterparts Dα2 and Dβ1 were described as potentially α-BGT interacting by affinity chromatography (Chamaon et al. 2002), indicating that insect α-BGT-sensitive receptors might be either homomeric and/or heteromeric depending whether they rely on α7 alone or in combination with additional α or β subunits (Thany et al. 2007), here α2 and/or β1. Both KC and AL cells might therefore express homo- and heteromeric nAChRs, supporting the hypothesis that different nAChR subsets can coexist within a same cell type as suggested in AL cells (Barbara et al. 2008; Nauen et al. 2001).

Comparison with pupal AL cell and KC nAChRs: developmental implications. The pharmacological profile of adult KC nAChRs is also similar to those of pupal AL cell and KC nAChRs previously described, which share sensitivities to the agonists

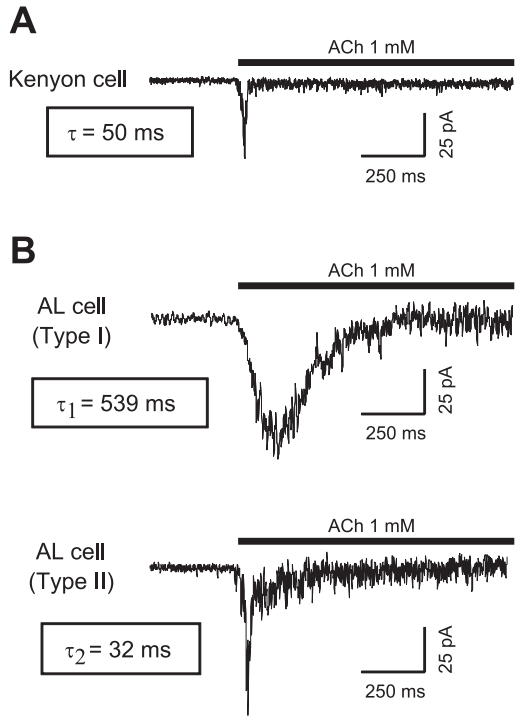

Fig. 5. Desensitization kinetics of AL cell and KC nAChRs. KC (*A*) and AL cell type I and type II (*B*) ACh-induced current desensitization was assessed through sustained application of 1 mM ACh (pulse duration 20 s, holding potential −110 mV), yielding time constant (τ) = 50.2 ± 4.6 ms (n = 13), τ = 539 ± 81 ms (n = 45), and τ = 32 ± 6 ms (n = 16), respectively (Barbara et al. 2008).

ACh, NIC, and IMI and to the antagonists DHE, MLA, and α-BGT (Barbara et al. 2005; Goldberg et al. 1999; Wüstenberg and Grünewald 2004). However, several differences between pupal and adult nAChRs can be pointed out, particularly when considering KCs. Adult KC ACh-elicited current mean peak amplitudes are much smaller than those previously recorded in pupal KCs (25.4 pA compared with 188 pA, respectively) and show a fivefold weaker affinity for ACh, as well as a fourfold weaker affinity for NIC, which is a full agonist in adult KCs but a partial agonist in pupal KCs (Wüstenberg and Grünewald 2004). Moreover, the antagonists DHE and MLA are strikingly more effective on pupal KC nAChRs than on their adult counterparts (5×10^6-fold and 2×10^3-fold, respectively). The pupal and adult KC nAChRs differ also in their permeability to calcium (Goldberg et al. 1999). Together, these results raise the question of whether some changes in subunit expression occur during development that explain the differences observed between receptors of the same cell type at distinct time points. Preliminary single-cell RT-PCR experiments performed on pupal KCs show varying expression profiles of nicotinic subunits comprising α2 alone or, less frequently, combined with α8 and/or β1 (J. P. Dupuis, unpublished observation), which is in good accordance with previous reports indicating that pupal KCs and AL cells show versatile expression patterns (Thany et al. 2005). Similar versatile expression patterns are observed in single-cell RT-PCR experiments performed on pupal AL cells, with the occasional supplementary expression of nicotinic subunits α7 and/or α3 (J. P. Dupuis, unpublished observation). Compared with the stable expression patterns observed in adult AL cells and KCs, these preliminary observations suggest that the expression profiles of nicotinic subunits might change considerably during development before reaching a stable state in adults.

Kinetic properties of nAChRs from adult honeybee AL cells and KCs: functional implications. Surprisingly, the ACh-induced currents recorded in KCs and AL cells appear to be strikingly different from a kinetic point of view. Whereas the majority type I AL nAChRs—which represent 90% of AL ACh-induced currents—are slow desensitizing (τ = 539 ms), KC nAChRs are fast desensitizing (τ = 50 ms) and resemble the minority type II ACh-induced currents observed in AL cells (τ = 32 ms) (Barbara et al. 2008). This result once again suggests structural and functional differences between nAChRs from KCs and AL cells, although changing regulatory mechanisms could also be involved. This hypothesis is reinforced by the observation that AL cells and KCs share similar subunit expression patterns except for the supplementary presence of α7 in AL cells, which could be responsible for these contrasted kinetic properties. Moreover, this dissimilarity between AL cell and KC nAChRs might also underlie functional implications and mirror successive levels of olfactory information processing. As in vertebrates, the olfac-

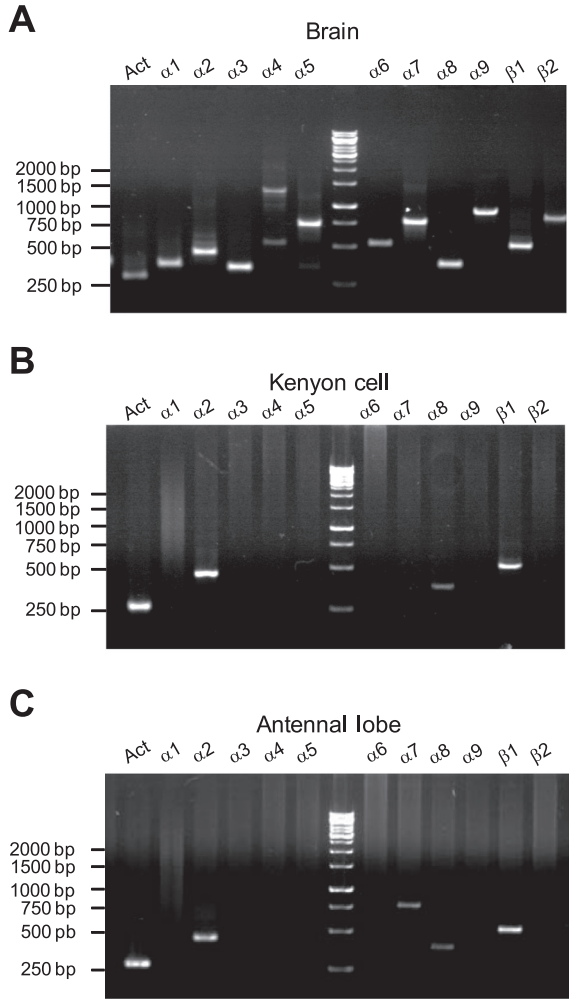

Fig. 6. Single-cell RT-PCR evidence for the expression of multiple nicotinic subunit mRNAs in mushroom bodies KCs and AL cells. Agarose gel analyses of representative entire honeybee brain (*A*), KC (*B*), and AL cell (*C*) are shown. KCs prove to be positive only for α2, α8, and β1 (n = 18), while AL cells are positive for α2, α7, α8, and β1 (n = 26) and the entire brain expresses all nicotinic subunit mRNAs present in the honeybee genome (α1–α9, β1, and β2). Actin (Act) was used as a positive control.

tory pathway of insects involves two main synapses separating the sensory periphery area and the higher-order brain centers, respectively located in the AL and the MBs or the lateral horn (Masse et al. 2009). Once spatiotemporally processed and synchronized in the AL, the odor-evoked stimulus is sent through PNs to the lateral horn and ultimately the KCs (Laurent et al. 1996; Müller et al. 2002). Interestingly, even though an important amount of olfactory information is sent through PNs, KCs remain weakly active, suggesting the existence of an important filter at the MB level requiring both proper signal timing between oscillatory activating inputs from PNs and inhibitory inputs from the lateral horn combined with specific intrinsic membrane properties of KCs (Grünewald 1999; Liu et al. 2007; Liu and Davis 2009; Perez-Orive et al. 2002). Our findings suggest that the fast-desensitizing properties of KC nAChRs could constitute one of the components of this complex synaptic integration at the KC level.

Further experiments using RNA silencing strategies will be required to unravel the precise contributions of each nicotinic subunit to AL and KC nAChRs and define the respective roles of each receptor subtype in olfactory processing. Together, our data provide the first picture of the molecular properties of nicotinic receptors in the honeybee olfactory neuropiles. They demonstrate that both molecular and electrophysiological features of nicotinic receptors differ in the AL and the MBs, where they could play successive roles in olfactory coding.

ACKNOWLEDGMENTS

We thank Dr. Marc Moreau and Dr. Catherine Leclerc for technical support.

Present address of J. P. Dupuis: CNRS UMR 5293, Institut des Maladies Neurodégénératives, Université Victor Segalen Bordeaux 2, Bât. 2A, 2ème étage, Case 22, 146 rue Léo Saignat, 33076 Bordeaux, France.

GRANTS

This work is part of the Apigene project supported by The University Paul Sabatier (Toulouse, France). J. P. Dupuis is the recipient of a postdoctoral grant from the Centre National de la Recherche Scientifique (CNRS).

DISCLOSURES

No conflicts of interest, financial or otherwise, are declared by the author(s).

REFERENCES

Albert JL, Lingle CJ. Activation of nicotinic acetylcholine receptors on cultured *Drosophila* and other insect neurones. *J Physiol* 163: 605–630, 1993.

Albuquerque EX, Pereira EF, Alkondon M, Rogers SW. Mammalian nicotinic acetylcholine receptors: from structure to function. *Physiol Rev* 89: 73–120, 2009.

Barbara GS, Zube C, Rybak J, Gauthier M, Grünewald B. Acetylcholine, GABA and glutamate induce ionic currents in cultured antennal lobe neurons of the honeybee, *Apis mellifera*. *J Comp Physiol A Neuroethol Sens Neural Behav Physiol* 191: 823–836, 2005.

Barbara GS, Grünewald B, Paute S, Gauthier M, Raymond-Delpech V. Study of nicotinic acetylcholine receptors on cultured antennal lobe neurones from adult honeybee brains. *Invert Neurosci* 8: 19–29, 2008.

Bicker G. Histochemistry of classical neurotransmitters in antennal lobes and mushroom bodies of the honeybee. *Microsc Res Tech* 45: 174–183, 1999.

Brandt R, Rohlfing T, Rybak J, Krofczik S, Maye A, Westerhoff M, Hege HC, Menzel R. Three-dimensional average-shape atlas of the honeybee brain and its applications. *J Comp Neurol* 492: 1–19, 2005.

Brown LA, Ihara M, Buckingham SD, Matsuda K, Sattelle DB. Neonicotinoid insecticides display partial and super agonist actions on native insect nicotinic acetylcholine receptors. *J Neurochem* 99: 608–615, 2006.

Cayre M, Buckingham SD, Yagodin S, Sattelle DB. Cultured insect mushroom body neurons express functional receptors for acetylcholine, GABA, glutamate, octopamine, and dopamine. *J Neurophysiol* 81: 1–14, 1999.

Chamaon K, Smalla KH, Thomas U, Gundelfinger ED. Nicotinic acetylcholine receptors of *Drosophila*: three subunits encoded by genomically linked genes can co-assemble into the same receptor complex. *J Neurochem* 80: 149–157, 2002.

Dacher M, Lagarrigue A, Gauthier M. Antennal tactile learning in the honeybee: effect of nicotinic antagonists on memory dynamics. *Neuroscience* 130: 37–50, 2005.

Déglise P, Grünewald B, Gauthier M. The insecticide imidacloprid is a partial agonist of the nicotinic receptor of honeybee Kenyon cells. *Neurosci Lett* 321: 13–16, 2002.

Dent JA. Evidence for a diverse Cys-loop ligand-gated ion channel superfamily in early bilateria. *J Mol Evol* 62: 523–535, 2006.

Dupuis JP, Bazelot M, Barbara GS, Paute S, Gauthier M, Raymond-Delpech V. Homomeric RDL and heteromeric RDL/LCCH3 GABA receptors in the honeybee antennal lobes: two candidates for inhibitory transmission in olfactory processing. *J Neurophysiol* 103: 458–468, 2010.

Farris SM, Sinakevitch I. Development and evolution of the insect mushroom bodies: towards the understanding of conserved developmental mechanisms in a higher brain center. *Arthropod Struct Dev* 32: 79–101, 2003.

Gauthier M, Dacher M, Thany SH, Niggebrugge C, Deglise P, Kljucevic P, Armengaud C, Grunewald B. Involvement of alpha-bungarotoxin-sensitive nicotinic receptors in long-term memory formation in the honeybee (*Apis mellifera*). *Neurobiol Learn Mem* 86: 164–174, 2006.

Goldberg F, Grünewald B, Rosenboom H, Menzel R. Nicotinic acetylcholine currents of cultured Kenyon cells from the mushroom bodies of the honey bee *Apis mellifera*. *J Physiol* 514: 759–768, 1999.

Grünewald B. Physiological properties and response modulations of mushroom body feedback neurons during olfactory learning in the honeybee, *Apis mellifera*. *J Comp Physiol A Neuroethol Sens Neural Behav Physiol* 185: 565–576, 1999.

Hamill OP, Marty A, Neher E, Sakmann B, Sigworth FJ. Improved patch-clamp techniques for high-resolution current recording from cells and cell-free membrane patches. *Pflügers Arch* 391: 85–100, 1981.

Hermsen B, Stetzer E, Thees R, Heiermann R, Schrattenholz A, Ebbinghaus U, Kretschmer A, Methfessel C, Reinhardt S, Maelicke A. Neuronal nicotinic receptors in the locust *Locusta migratoria*: cloning and expression. *J Biol Chem* 273: 18394–18404, 1998.

Hogg RC, Raggenbass M, Bertrand D. Nicotinic acetylcholine receptors: from structure to brain function. *Rev Physiol Biochem Pharmacol* 147: 1–46, 2003.

Honeybee Genome Sequencing Consortium. Insights into social insects from the genome of the honeybee *Apis mellifera*. *Nature* 443: 931–949, 2006.

Ihara M, Matsuda K, Otake M, Kuwamura M, Shimomura M, Komai K, Akamatsu M, Raymond V, Sattelle DB. Diverse actions of neonicotinoids on chicken alpha7, alpha4beta2 and *Drosophila*-chicken SADbeta2 and ALSbeta2 hybrid nicotinic acetylcholine receptors expressed in *Xenopus laevis* oocytes. *Neuropharmacology* 45: 133–144, 2003.

Jepson JE, Brown LA, Sattelle DB. The actions of the neonicotinoid imidacloprid on cholinergic neurons of *Drosophila melanogaster*. *Invert Neurosci* 6: 33–40, 2006.

Jones AK, Sattelle DB. The cys-loop ligand-gated ion channel superfamily of the honeybee, *Apis mellifera*. *Invert Neurosci* 6: 123–132, 2006.

Jones AK, Raymond-Delpech V, Thany SH, Gauthier M, Sattelle DB. The nicotinic acetylcholine receptor gene family of the honey bee, *Apis mellifera*. *Genome Res* 16: 1422–1430, 2006.

Jones AK, Sattelle DB. The cys-loop ligand-gated ion channel gene superfamily of the red flour beetle, *Tribolium castaneum*. *BMC Genomics* 8: 327, 2007.

Kelber C, Rossler W, Kleineidam CJ. Multiple olfactory receptor neurons and their axonal projections in the antennal lobe of the honeybee *Apis mellifera*. *J Comp Neurol* 496: 395–405, 2006.

Kreissl S, Bicker G. Dissociated neurons of the pupal honeybee brain in cell culture. *J Neurocytol* 21: 545–556, 1992.

Lapied B, Le Corronc H, Hue B. Sensitive nicotinic and mixed nicotinic-muscarinic receptors in insect neurosecretory cells. *Brain Res* 533: 132–136, 1990.

Laurent G, Wehr M, Davidowitz H. Temporal representations of odors in an olfactory network. *J Neurosci* 16: 3837–3847, 1996.

Liu X, Krause WC, Davis RL. $GABA_A$ receptor RDL inhibits *Drosophila* olfactory associative learning. *Neuron* 56: 1090–1102, 2007.

Liu X, Davis RL. The GABAergic anterior paired lateral neuron suppresses and is suppressed by olfactory learning. *Nat Neurosci* 12: 53–59, 2009.

Lozano VC, Armengaud C, Gauthier M. Memory impairment induced by cholinergic antagonists injected into the mushroom bodies of the honeybee. *J Comp Physiol A* 187: 249–254, 2001.

Masse NY, Turner GC, Jefferis GS. Olfactory information processing in *Drosophila*. *Curr Biol* 19: R700–R713, 2009.

Müller D, Abel R, Brandt R, Zockler M, Menzel R. Differential parallel processing of olfactory information in the honeybee, *Apis mellifera L. J Comp Physiol A Neuroethol Sens Neural Behav Physiol* 188: 359–370, 2002.

Nauen R, Ebbinghaus-Kintscher U, Schmuck R. Toxicity and nicotinic acetylcholine receptor interaction of imidacloprid and its metabolites in *Apis mellifera* (Hymenoptera: Apidae). *Pest Manag Sci* 57: 577–586, 2001.

Papke RL, Porter Papke JK. Comparative pharmacology of rat and human α7 nAChR conducted with net charge analysis. *Br J Pharmacol* 137: 49–61, 2002.

Perez-Orive J, Mazor O, Turner GC, Cassenaer S, Wilson RI, Laurent G. Oscillations and sparsening of odor representations in the mushroom body. *Science* 297: 359–365, 2002.

Raymond V, Sattelle DB. Novel animal-health drug targets from ligand-gated chloride channels. *Nat Rev Drug Discov* 1: 427–436, 2002.

Salgado VL, Saar R. Desensitizing and non-desensitizing subtypes of alpha-bungarotoxin-sensitive nicotinic acetylcholine receptors in cockroach neurons. *J Insect Physiol* 50: 867–879, 2004.

Schulz R, Bertrand S, Chamaon K, Smalla KH, Gundelfinger ED, Bertrand D. Neuronal nicotinic acetylcholine receptors from *Drosophila*: two different types of alpha subunits coassemble within the same receptor complex. *J Neurochem* 74: 2537–2546, 2000.

Shimomura M, Satoh H, Yokota M, Ihara M, Matsuda K, Sattelle DB. Insect-vertebrate chimeric nicotinic acetylcholine receptors identify a region, loop B to the N-terminus of the *Drosophila* Dalpha2 subunit, which contributes to neonicotinoid sensitivity. *Neurosci Lett* 385: 168–172, 2005.

Strausfeld NJ. Organization of the honey bee mushroom body: representation of the calyx within the vertical and gamma lobes. *J Comp Neurol* 450: 4–33, 2002.

Thany SH, Crozatier M, Raymond-Delpech V, Gauthier M, Lenaers G. Apisalpha2, Apisalpha7–1 and Apisalpha7–2: three new neuronal nicotinic acetylcholine receptor alpha-subunits in the honeybee brain. *Gene* 344: 125–132, 2005.

Thany SH, Lenaers G, Raymond-Delpech V, Sattelle DB, Lapied B. Exploring the pharmacological properties of insect nicotinic acetylcholine receptors. *Trends Pharmacol Sci* 28: 14–22, 2007.

Vermehren A, Trimmer BA. Expression and function of two nicotinic subunits in insect neurons. *J Neurobiol* 62: 289–298, 2005.

Wüstenberg DG, Grünewald B. Pharmacology of the neuronal nicotinic acetylcholine receptor of cultured Kenyon cells of the honeybee, *Apis mellifera*. *J Comp Physiol A Neuroethol Sens Neural Behav Physiol* 190: 807–821, 2004.